

A semi-supervised approach to segment the retinal blood vessels in color fundus photographs

Md. Abu Sayed

Tanmai Kumar Ghosh



**Computer Science and Engineering Discipline
Khulna University
Khulna-9208, Bangladesh
December, 2018**

A semi-supervised approach to segment the retinal blood vessels in color fundus photographs

Md. Abu Sayed

(Student ID: 150220)

Tanmai Kumar Ghosh

(Student ID: 150232)

SUBMITTED IN PARTIAL FULFILLMENT OF THE REQUIREMENTS FOR THE DEGREE BACHELOR
OF SCIENCE IN COMPUTER SCIENCE AND ENGINEERING

AT

Computer Science and Engineering Discipline

Khulna University

Khulna-9208, Bangladesh

December, 2018

Khulna University
Computer Science and Engineering Discipline

The undersigned hereby certify that they have read and recommended to the Computer Science and Engineering Discipline for acceptance of a thesis entitled “**A semi-supervised approach to segment the retinal blood vessels in color fundus photographs**” by **Md. Abu Sayed and Tanmai Kumar Ghosh** in partial fulfillment of the requirements for the degree **Bachelor of Science in Computer Science and Engineering (CSE)**.

Dated: January 22, 2019

Dr. G.M. Atiqur Rahaman

Professor

Computational Color & Spectral Image Analysis Lab.
Computer Science and Engineering Discipline,
Khulna University, Khulna-9208.

Thesis Supervisor

Dr. Sajib saha

Research Scientist

Australian E Health Research Centre,
Commonwealth Scientific and Industrial Research Organization (CSIRO), Australia

Thesis Co-supervisor

S M Mohidul Islam

Assistant Professor

Computer Science and Engineering Discipline,
Khulna University, Khulna-9208.

Thesis External

Dr. Md. Anisur Rahman

Professor

Computer Science and Engineering Discipline,
Khulna University, Khulna-9208.

Head of the Discipline

Abstract

Segmentation of retinal blood vessels is very important diagnostic procedure in ophthalmology. Segmenting blood vessels in presence of pathological lesion is one of the major challenges while segmentation. In this thesis, we propose a method to segment retinal blood vessel to overcome this challenge. The proposed method is also able to overcome the most of the other challenges such as segmentation in presence of central vessel reflex, crossover and bifurcation regions etc. We evaluate the proposed method on three publicly available and popular dataset: DRIVE, STARE and CHASE_DB1. We get promising performance for each of the dataset. For DRIVE dataset, the Accuracy, Area Under Curve (AUC), Sensitivity, Specificity are 0.961, 0.847, 0.711 and 0.983 respectively. For STARE dataset, they are 0.960, 0.878, 0.790 and 0.973 respectively and for CHASE_DB1 they are 0.951, 0.854, 0.742 and 0.967. To extract trainable feature, we propose a descriptor and compare the descriptor with a novel descriptor (SURF). We get nearly identical performance for the proposed descriptor respect to SURF descriptor.

Acknowledgement

At first we are extremely grateful to almighty Allah for giving us patience to perform our thesis implementation properly. We would like to express our sincere gratitude to our supervisor Dr. G.M. Atiqur Rahaman, Professor, Computer Science and Engineering Discipline, Khulna University and co-supervisor Dr. Sajib Saha, Research Scientist, Australian E Health Research Centre, Commonwealth Scientific and Industrial Research Organization (CSIRO), Australia for their constant and kind guidance and encouragement which ultimately assisted us to complete our thesis successfully.

We also highly grateful to our external S.M. Mohidul Islam, Assistant Professor, Computer Science and Engineering Discipline, Khulna University. He has given us the scope, necessary encouragement and his valuable suggestion for completing the thesis work in a timely manner.

Khulna

Md. Abu Sayed
Tanmai Kumar Ghosh

Contents

Title Page	i
Submission Page	ii
Abstract	iii
Acknowledgement	iv
Table of Contents	v
List of Tables	vi
List of Figures	vii
1 Introduction	1
2 Literature Review	4
3 Materials and Methods	7
3.1 Supporting Methods	7
3.1.1 Multi-scale Line Detector	7
3.1.2 The SURF Descriptors	9
3.1.3 Random Forest Classifier	9
3.2 Datasets	11
3.2.1 DRIVE Dataset	11
3.2.2 STARE Dataset	11
3.2.3 CHASE_DB1 Dataset	12
3.3 Performance Measurements	12
4 Proposed Methodology	14
4.1 Initial Segmentation	15
4.1.1 Preprocessing	15
4.1.2 Segmentation of retinal image by Multi-scale Line detector	15
4.2 Proposed Approach	17

4.2.1	Local Haar Pattern (LHP)	18
4.2.2	Training Phase	20
4.2.3	Test Phase	21
5	Results and Comparisons	24
5.1	Model Evaluation on DRIVE Dataset	24
5.2	Model evaluation on STARE dataset	24
5.3	Model evaluation on CHASE_DB1 dataset	24
6	Conclusion	33

List of Tables

3.1	Performance Measurement Parameters	12
5.1	Performance results of DRIVE dataset	25
5.2	Performance results of STARE dataset	26
5.3	Performance results of CHASE_DB1 dataset	27
5.4	Performance comparison on DRIVE and STARE datasets	28
5.5	Comparative performance of Descriptors	32

List of Figures

1.1	The normal images from DRIVE dataset	2
1.2	Types of Diabetic Retinopathy	2
2.1	Pathology and false vessel detection	6
4.1	Overview of the proposed method	14
4.2	Sample image from DRIVE dataset	15
4.3	Resulting image after applying line with varying length	16
4.4	: Output of Multi-scale Line Detector	16
4.5	Drawbacks of Multi-scale Line Detector	17
4.6	All 16 Patterns for feature extraction in LHP	18
4.7	Decomposition of main patch into sub-patches	19
4.8	Training Phase	21
4.9	Test Phase	22
4.10	Sample output of Proposed Method (LPH descriptor)	23
5.1	Performance comparison on DRIVE dataset (Supervised)	29
5.2	Performance comparison on DRIVE dataset (Un-supervised)	30
5.3	Performance comparison on Stare dataset (Supervised)	30
5.4	Performance comparison on Stare dataset (Un-supervised)	31
5.5	Performance comparison of proposed and Nyugen et al.	31

Chapter 1

Introduction

Diabetes occurs when the body can't use the insulin effectively produced by the pancreas or the pancreas can't produce the insulin the body needs. Insulin is a kind of hormone generated by beta cells in the pancreas. Insulin controls the level of blood sugar. Diabetic also known as Diabetes Mellitus (DM) causes a serious eye disease which is called Diabetic Retinopathy (DR). DR has two different stages. One is (1) Proliferative DR (PDR) and another is (2) non-proliferative DR (NPDR) [1]. NPDR contains Microaneurysms (MAs), Exudates (EXs) and Hemorrhages (HMs). The abnormal growth of retinal blood vessels in retina refers to Proliferative Diabetic Retinopathy (PDR) [1]. The normal images of retina are shown in 1.1 . In this figure, no abnormalities are noticed. The affected images are shown in 1.2. In this figure, the first and the second image show the signs of Non-proliferative and proliferative diabetic retinopathy respectively. Microaneurysms (MAs) are the earliest sign of DR [2]. MAs appear as small, round

and dark dots on the retinal surface [2]. They have sharp margins. For the leakage of weak capillaries causes Hemorrhages (HAs) [2]. Normally, they have various shapes like flame, dot and blot. HAs are defined as the red spots uneven edges and coloring [2]. Microaneurysms that appear as white dots with no blood visible in the lumen are considered hard exudates. They are a kind of lipoprotein. HEs are small white or yellowish white deposits with irregular shapes, sharp edges [2]. The abnormal growth of blood vessels called Neovascularization on the inner surface of the retina is the symptom of proliferative diabetic retinopathy. It is the advance stage of diabetic retinopathy.

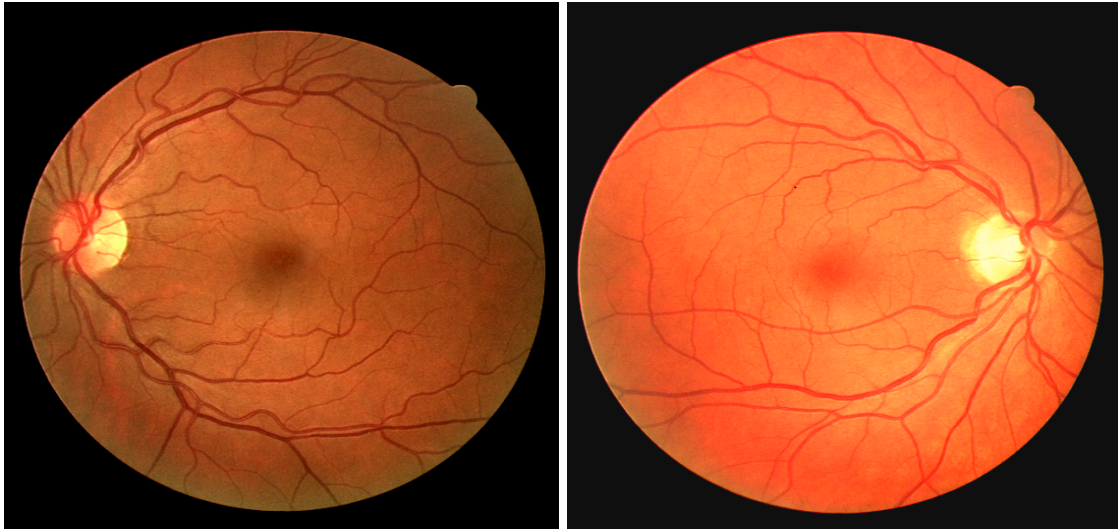
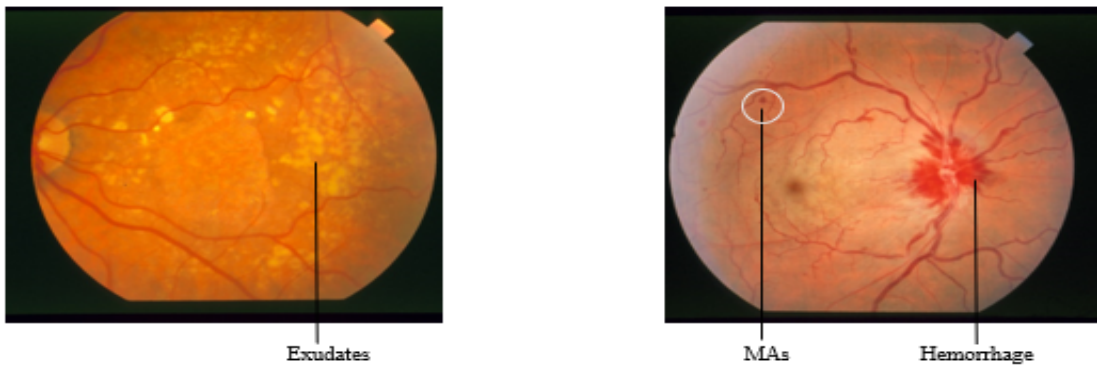


Figure 1.1: The normal images from DRIVE dataset



(a) Non-Proliferative DR



(b) Proliferative Diabetic Retinopathy

Figure 1.2: Types of Diabetic Retinopathy

Change in any feature of retinal image such as shape, branching pattern, tortuosity and width is the precautions of many serious diseases such as cardiovascular diseases, Stroke, Diabetic Retinopathy (DR), Glaucoma and Age-related Macular Degeneration (ARMD) [3]. In fact, DR is one of the main reasons for blindness in the developed country. About 80 percent people having diabetes mellitus are affected by Diabetic retinopathy for 20 years or more [5]. Detection of diabetic retinopathy in early age is very important for preventing blindness. To this end, Automatic Screening System is required for diagnosis of Diabetic Retinopathy and other vascular diseases by analyzing the changing features of blood vessels in retinal images. Thus, an accurate segmentation of retinal blood vessels is very important for the screening system. The segmentation of blood vessels from retinal image is very challenging and important task for automatic diagnosis of Diabetic Retinopathy and other vascular diseases. It is required to automatically detect the abnormalities of retinal images which is discussed above. Also, vessel segmentation is of great significance in case of developing technique to detect and analyze diseases relevant to the vessels (example, Neo-Vascularization). For the last two decades, a significant amount of research has been done for segmenting retinal blood vessels. Still there are scopes for contributing in this field. There are a number of challenges while segmenting retinal blood vessels. The challenges are given below [4]:

1. Segmenting retinal blood vessels in the presence of central vessel reflex.
2. Segmenting blood vessels presenting in crossover and bifurcation regions.
3. Segmenting the merging of close vessels.
4. Segmenting the small and thin vessels.
5. Segmenting the blood vessels in the pathological region (Dark lesion and bright legion).

Addressing these challenges are required for obtaining correct segmentation results. In this thesis, we proposed a method to segment the retinal blood vessels in color fundus photographs. The main contribution is to improve an existing method that produces incorrect segmentation results in presence of various Diabetic Retinopathies.

Chapter 2

Literature Review

A number of researches have been done for segmenting retinal blood vessels. We briefly discuss the state-of-the-art paper. Supervised and unsupervised are two methods found

in the literature for segmenting retinal blood vessels. A set of training images are required for supervised methods that are manually labeled by specialists for classifying a pixel either as vessel or a non-vessel [6]. There are many supervised methods introduced in the literature for segmenting retinal blood vessels. On the other hand, unsupervised method does not require any annotated label. Most of the methods of the unsupervised learning are based on the basic image processing techniques such as mathematical morphology, matched filters, thresholding, vessel tracing, region growing, multiscale purposes etc. We proposed a semi-supervised method for the segmentation of retinal blood vessels. Wang et al [7] proposed a segmentation method based on

matched filter. In this method vessels are enhanced using matched filtering with multiwavelet kernels (MFMK). Multiscale hierarchical decomposition method was used to remove noise and locate the vessel. The method proposed by Wang et al is successful for the wavelet kernels. For detecting the edges of blood vessels borders, wavelet kernels are especially suitable. The method is implemented on the DRIVE and STARE database. The accuracy of the method is 0.9461 and 0.9521 for DRIVE and STARE database respectively. Das et al. [8] proposed a thresholding-based technique for segmenting retinal

vessels. The paper includes three steps for segmentation: (1) preprocessing; (2) segmentation; (2) postprocessing. For preprocessing, Contrast limited adaptive histogram equalization is used which enhances the quality of retinal image. Mean-c clustering method is used for segmentation to extract retinal blood vessels. Mathematical morphology is used for postprocessing which removes the isolated pixels. The proposed method can't segment the pathological lesions and the optic disk. The accuracy of this method for DRIVE and CHASE_DB (Child heart and health study in England) dataset is 0.955 and 0.954 respectively. Yang et al [9] proposed a method for segmentation of retinal

blood vessel based on mathematical morphology and a fuzzy clustering algorithm.

Mathematical morphology is used for Preprocessing which increases the smoothness and strength of the retinal image. Then, fuzzy clustering algorithm is applied to pre-processed image for segmentation of retinal image. To reduce the noise and weak edges purification is done. Finally, the segmented blood vessels are achieved. Wang et al.

[10] proposed a blood vessels segmentation method based on the feature and ensemble learning. The CNN is used for extracting trainable hierarchical feature and ensemble RFs work as trainable classifier. Two publicly available database DRIVE and STARE are used for comparing the result. Marin et al [11] proposed a supervised method for reti-

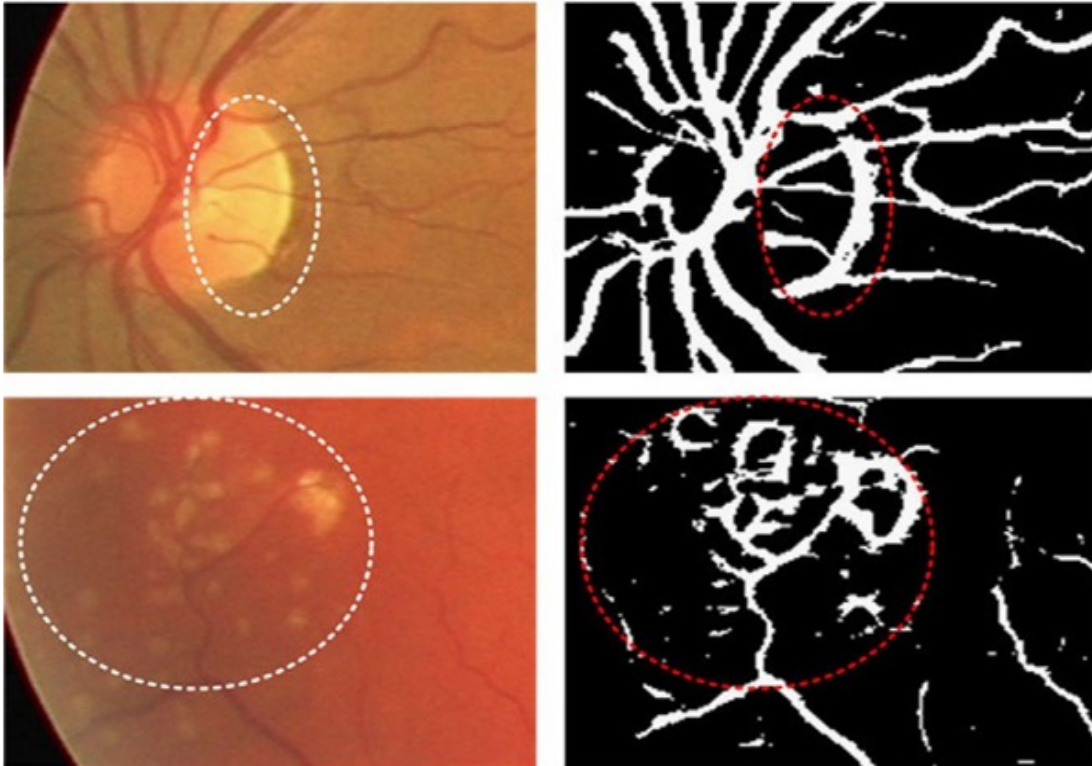
nal blood vessels segmentation based on Neural Network (NN) and pixel classification using 7-D feature vector. The 7-D feature vector are extracted from the preprocessed retinal images. To classify each pixel as vessel or non-vessel, classification results (real values between 0 and 1) are generated by threshold. Ricci et al [12] proposed a segmen-

tation method based on basic line operators and support vector machine. Line detection is used to determine the discontinuity of intensity value of an image. The green channel is extracted from the original retinal image. Because, green channel has less noise and better illumination. The red or blue channel is more prone to noise. They have also poor illumination than green channel. Basic line detector deals with inverted green channel. In inverted green channel, the vessels appear brighter than the background. A window of $W \times W$ is taken for each pixel position. The method has limitations such as it has poor segmentation result in the presence of central vessel reflex, at bifurcation and crossover regions, the possibility of merging close vessels. For solving the limitations, Nguyen et al [4] proposed a method based on the line detector of varying length upon which our proposal is built Nguyen et al [4] proposed a method based on multiscale

detection. The method is the modification of the method proposed by the Ricci et al [12]. The advantage of the method is no preprocessing is required for segmentation. The Method can segment the vessels:

1. In presence of central vessel reflex (CVF).
2. At bifurcation and crossover regions.
3. In presence of merging of close vessels.

But the method is unable to segment the small and tinny vessels. The method can't segment the blood vessels in presence of pathological lesions and optic disk which is shown in figure 2.1.



a) First column contains the portions of optic disk and pathological lesions in original image [3]

b) Second column contains the segmented false vessels [4].

Figure 2.1: Pathology and false vessel detection

Chapter 3

Materials and Methods

3.1 Supporting Methods

The methodologies that we use to implement proposed method are described as follows.

3.1.1 Multi-scale Line Detector

Multi-scale line detector is based on the basic line detector. We first describe the basic line detector, then describe the multi-scale line detector. The basic line detector deals

with the inverted green channel of a retinal image. In inverted green channel of retinal image, the vessels appear brighter than the background. A window of size $W \times W$ is taken at each pixel position. Then the average gray level is computed as I_{avg}^w . Twelve lines of length W pixels oriented at twelve different directions of 15° angular difference is taken [4]. The lines pass through the centered pixel and average gray level of each line is calculated. Then the line with maximum average value called ‘winning line’ is identified and defined as I_{max}^w . The line response at a pixel is calculated as follows [4]:

$$R_W = I_{max}^w - I_{avg}^w \quad (3.1)$$

If the response value of the pixel is large (larger than zero), then the pixel is defined as vessel. Otherwise, the pixel is non-vessel. There is only one parameter in basic line detector which is the window size, w . The window size, w at each pixel is chosen in such a way that there are approximately equal number of vessels and background pixels. That is, the window size, w is set twice of the vessel’s width in an image set. For example, $W=15$ is perfect choice for DRIVE [3] dataset as the vessels width of the dataset is typically 7-8 pixels [12]. The basic line detector is very effective dealing with vessel central light reflex [12]. There are three disadvantages of basic line detector including [4]:

1. It tends to merge close vessels.

2. It produces an extension at crossover points.
3. It produces false vessel responses at background pixels near strong vessels.

To overcome the three drawbacks mentioned above, multi-scale line detector is used. It is the generalization of basic line detector by varying the length of the aligned lines. The generalized line detector is defined as follows [4]:

$$R_W^L = I_{max}^L - I_{avg}^L \quad (3.2)$$

Here, I_{max}^L is the value of winning line (the line with maximum average value), I_{avg}^L is the average intensity value of the window. R_W^L is the raw response value of the centered pixel of the window. The value of length, L ranges from one to window size. Line detectors at different scales are achieved by varying the length of L . The reason of varying the length of line is the shorter lengths will avoid the inclusion of surrounding vessel pixels. That is, multi-scale line detector provides correct response value which solves three drawbacks mentioned above. The raw response values provided by line detector are in very low range at each scale. As a result, there is a low contrast between vessels and the background. We have to standardize the values of the raw response to make it have zero mean and unit standard deviation standard distribution [4]:

$$R' = \frac{R - R_{mean}}{R_{SD}} \quad (3.3)$$

Where R' is the standardize response value, R is the raw response value, R_{mean} and R_{SD} are the mean and standard deviation of the raw response values, respectively.

As a result of reducing the line length, it can be noticed that background noise is introduced in the whole image. Line responses at varying scales are linearly combined to overcome the problem. The combination process has been done by following equation [4]:

$$R_{com} = \frac{1}{n_L} \left(\sum_L R_W^L + I_{igc} \right) \quad (3.4)$$

Where n_L is the number of scales used, R_W^L is the response of line detector at scale of L , I_{igc} is the value of inverted green channel at the corresponding pixel and R_{com} is the combined response value. The decision (the pixel is vessel or non-vessel) will be taken according the value of response. If the response value is relatively large, the pixel is vessel. Otherwise, it is considered as non-vessel.

3.1.2 The SURF Descriptors

There are many feature descriptors available for feature extraction with higher speed and accuracy. Scale Invariant Feature Transform (SIFT) [13], Speeded-Up Robust Features (SURF) [14], Opponent SIFT descriptors are significant among them.

SURF uses integral images and efficient scale space construction for generating key-points and descriptors effectively. SURF works on two stages: (1) key-point detection and (2) key-point description [15]. Integral image is very important while detecting the interest points. Integral image can be found as follows [14]:

$$S(x, y) = \sum_{i=0}^x \sum_{j=0}^y I(i, j) \quad (3.5)$$

Here $S(x, y)$ represents the summation of all pixels of input image I within a rectangular region initiated by the location (x, y) and the origin .

In the first stage, integral image helps the first computation of approximation of Laplacian of Gaussian (LoG) using a box filter. To detect the key-points, determinants of the Hessian matrix are calculated and used as a measure of local change around the point. The point is chosen based on the value of determinant. If the value of determinant is maximum, then the point is chosen [14]. The Hessian matrix $H(p, s)$ at point $p(x, y)$ and scale s in an image I is calculates as follows [14]:

$$H(p, s) = \begin{pmatrix} L_{yx}(p, s) & L_{xy}(p, s) \\ L_{yx}(p, s) & L_{xy}(p, s) \end{pmatrix} \quad (3.6)$$

In the second stage, each detected key-point is first assigned a fixed orientation. By creating a square window centered around the key-point and oriented along the orientation achieved before, the SURF descriptor is computed. The window is divided into 4×4 sub-regions. Then Haar wavelet of size $2s$ are calculated within each sub-region, where s is the size of scale. Each sub-region provides 4 values. Thus, SURF provides 64D descriptors vectors. Finally, the values are normalized to unit length.

In the proposed method, we use SURF descriptor to compare with our proposed Descriptor

3.1.3 Random Forest Classifier

The Random Forest Classifier (RFC) is a supervised method that is used to ensemble random binary decision trees which are created recursively. There is a combination of tree classifiers in the random forest classifier. The working procedure of random forest classifier is as follows [16]:

1. Training:

Let a training set has d tuples. The process of constructing n decision trees is described as flows: For each iteration, i , here $i = (1, 2, \dots, n)$, A training set (D_i) of d tuples is generated by sampling with replacement from D . For example, sample size $\frac{2}{3}$ of d . The

number of attributes is randomly selected that is used for determining the split of each node. Suppose, F be the number of randomly selected attributes. F can be calculated as $F = \log_2 N + 1$, where N is the total number of attributes. A decision tree classifier, M_i , is constructed by growing each tree. To grow each tree, the CART (classification and regression tree) methodology is used

2. Testing:

The maximum voted tree is the winner and thus, this is the output class of Random Forest (RF) classifier.

Attribute selection measure is used while designing the decision tree. There are many approaches for the selection of attributes used for decision tree induction. To select attribute, the CART methodology uses Gini index [16]. For a given training data set, Gini index is defined as follows:

$$Gini(D) = 1 - \sum_{i=1}^m p_i^2 \quad (3.7)$$

Where D is the value of an attribute, m is the number of class and p_i is the probability of class. The attribute selection is done by the following equation:

$$Gini_{SA}(D) = \sum_{c \in SA} p(c) Gini(c) \quad (3.8)$$

Where $Gini_{SA}(D)$ is the summation of probability of each attribute value multiplied by corresponding Gini index. The value indicates which attribute will be selected for decision tree induction. The attribute having smallest value is decided as winner and selected for tree induction.

Reasons of selecting Random Forest Classifier [10] in implementing the proposed method:

1. On large datasets, it can work efficiently.
2. Even in presence of noisy features, it is relatively robust.

3.2 Datasets

A special type of camera is used to capture the images of retina. The camera is called fundus camera. The images taken by fundus camera are called Retinal fundus image (RFI). Retinal fundus camera captures the images of the internal surface of the retina, macula, blood vessels and posterior pole [6]. Acquisition of image is a very crucial stage for medical diagnosis. Fortunately, eight datasets of retinal image are publicly available. They are DRIVE, STARE, CHASE_DB, DIARETDB, e-aphtha, HEIMED, Retinopathy Online Challenge (ROC), and MESSIDOR [6]. Our proposed method is evaluated on three publicly available datasets: DRIVE, STARE and CHASE_DB.

3.2.1 DRIVE Dataset

DRIVE [3] database was prepared in The Netherlands from a diabetic retinopathy screening program. There were 400 people affected by diabetic between 25-90 years of age. Canon CR5 non-mydratic 3 CCD camera with a 45-degree field of view (FOV) were used to acquire the images. Resolution of each image is 768×584 and the images are captured using 8 bits per color plane [3]. In DRIVE database there are 40 images which were randomly selected by the specialists. Among them 33 images don't show any symptom of Diabetic Retinopathy and rest of 7 images showed the symptom of early diabetic retinopathy. The all 40 images of DRIVE database are in JPEG format [3]. The images of DRIVE database have been divided into two sets. One is called training set and another is called test set. Each of the set contains 20 images [3]. However, training set contains 4 pathological images and test set contains 3 pathological images. The images of both training and test set have manual segmented image (Ground truth) image labeled by two individual observers.

3.2.2 STARE Dataset

STARE (Structured Analysis of the Retina) [17] contains 20 images for the segmentation of blood vessels. Among them ten images contain pathology and ten images are normal. There is no separate set of training and test images in STARE dataset. The images are achieved by a Tapcon [17] TRV-50 fundus camera at 35° field of view (FoV). The size of the images is 605×700 pixels, 8 bits per color channel. Two observers manually segmented (ground truth) all the images. The segmentation of the first observer is usually used as ground truth [17].

3.2.3 CHASE_DB1 Dataset

CHASE_DB1 [18] consists of 28 fundus images acquired from multiethnic school children. A hand-held Nidek NM-200-D fundus camera is used to capture the images at 30° field of view (FoV). And the size of each image is 960 × 999 pixels [18]. Two individual observers labeled the images of the dataset.

3.3 Performance Measurements

Every pixel is classified either as vessel or non-vessel (background, pathology, optic disc, macula etc.) in the retinal vessel segmentation process. There are four possible classification results: (1) true positive and (2) true negative (3) false positive and (4) false negative [19]. True positive (TP) refers to a pixel classified as vessel in both in the ground truth and the segmented image, while false positive (FP) refers to a pixel is classified as a vessel in segmented image but it is recognized as a non-vessel in the ground truth. True negative (TN) refers to a pixel classified as non-vessel in both in the ground truth and the segmented image, while false negative (FN) refers to a pixel classified as a non-vessel in segmented image but is recognized as a vessel in the ground truth.

Four events of vessel classification are shown in table 3.1 [19]:

	Vessel present	Vessel absent
Vessel detected	True Positive (TP)	False Positive (FP)
Vessel not detected	False Negative (FN)	True Negative (TN)

Table 3.1: Performance Measurement Parameters

Three common measurements are used in order to evaluate the performance of the vessel segmentation methods [19]. They are defined as follows:

$$Sensitivity = \frac{TP}{TP + FN} \quad (3.9)$$

$$Specificity = \frac{TN}{TN + FP} \quad (3.10)$$

$$Accuracy = \frac{TP + TN}{TP + TN + FP + FN} \quad (3.11)$$

Sensitivity (Se) specifies the ability of detecting vessel pixels of a method and speci-

ficity (Sp) refers the ability of detecting non-vessel pixels of a method. Accuracy (Acc) is a global measure of classification performance combining both Sensitivity and Specificity. Area under a receiver operating characteristics (ROC) curve (AUC) is also used to measure the performance of vessel segmentation method [19]. The conventional AUC is calculated from a number of operating points [19]. Normally, AUC is used to evaluate balanced data classification problem.

But blood vessel segmentation is an unbalanced data classification problem as there are fewer vessel pixels than background pixels in a retinal image [19]. The performance of vessel segmentation can be evaluated by applying the following formula [19]:

$$AUC = \frac{\text{Sensitivity} + \text{Specificity}}{2} \quad (3.12)$$

The higher value of Se, Sp, Acc, AUC refers that the method is better than other methods.

Chapter 4

Proposed Methodology

In the proposed method, multi-scale line detector is used to get an initially segmented image. Then, we extract the trainable feature from the retinal image by using a descriptor which is discussed in section 4.2.1. After that, Random Forest (RF) model is used as binary classifier to classify the pixel as vessel or non-vessel. So, the proposed method is divided into two phases. In the first phase, unsupervised multi-scale line detector will be applied for initial segmentation. In the second phase, supervised approach will be used to build classification model based on training image set. The following diagram gives a basic idea of the proposed method:

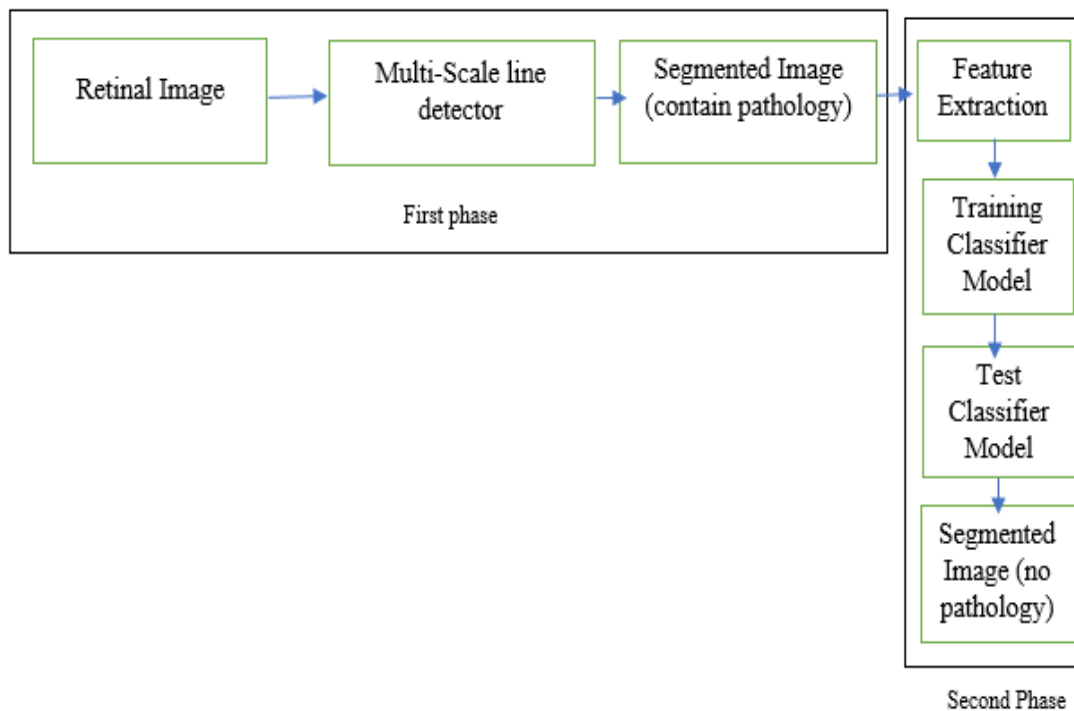


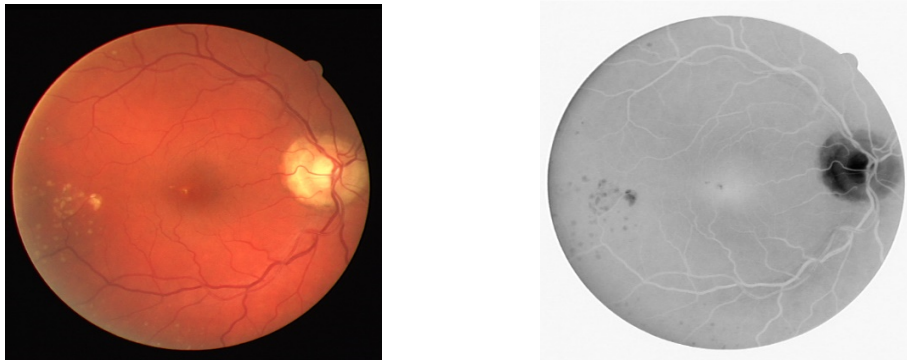
Figure 4.1: Overview of the proposed method

4.1 Initial Segmentation

We perform preprocessing and segmentation of the retinal image that contains false vessels in presence of pathological lesions.

4.1.1 Preprocessing

The green channel shows the best vessel-background contrast for colored images in RGB space, the red and blue channels show low contrast which is very noisy. The multi-scale line detector, therefore, works on the inverted green channel where the vessels appear brighter than the background [4]. Hence, we separate the green channel from the retinal image. Then the green channel is inverted by subtracting the green channel from 1. The image of inverted green channel from DRIVE dataset is shown in Figure 4.2.



1. Original Image 2. Inverted green channel

Figure 4.2: Sample image from DRIVE dataset

4.1.2 Segmentation of retinal image by Multi-scale Line detector

We apply multi-scale line detector [4] for the initial segmentation of the retinal image. Then the raw response value is calculated for the varying length of line. The raw response values provided by line detector are in very low range at each scale. As a result, there is a low contrast between vessels and the background. We have to standardize the values of the raw response to make it have zero mean and unit standard deviation standard distribution [4]. As a result of reducing the line length, it can be noticed that background noise is introduced in the whole image. Figure 4.3 shows the result of reducing the line length. In this figure, we notice that there is background noise. Line responses at varying scales are linearly combined to overcome the problem. The output of multi-scale line detector is shown in Figure 4.4. The details working procedure of multi-scale detector has been discussed in section 3.1.

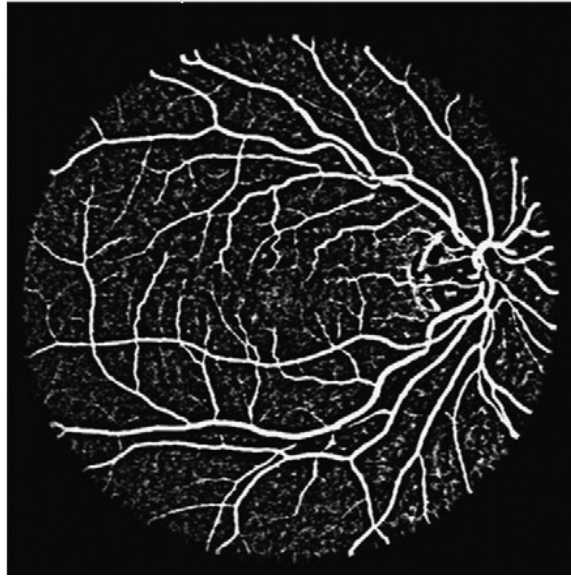
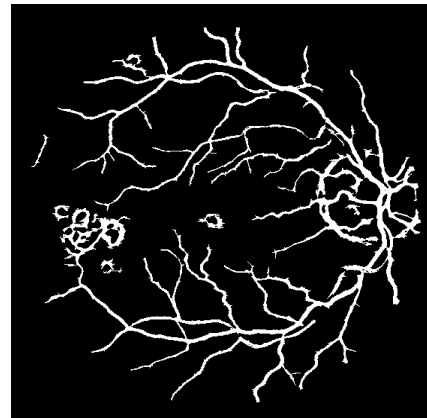


Figure 4.3: Resulting image after applying line with varying length



1. Original Image



2. Segmented Image

Figure 4.4: : Output of Multi-scale Line Detector

The drawback of multi-scale line detector is that it is unable to produce correct segmentation result in presence of Pathological lesions such as Microaneurysms (MAs), Exudates (EXs) and Hemorrhages (HMs).

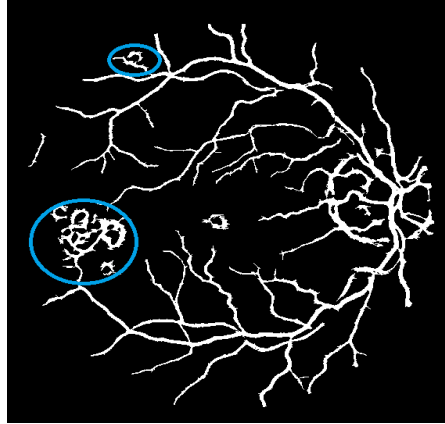


Figure 4.5: Drawbacks of Multi-scale Line Detector

In figure 4.5, the circular regions indicate the false vessels detected by multi-scale detector. However, false vessels segmentation in presence of pathological lesion may lead to inaccurate result while diagnosis of vascular diseases. That is, it is very important to improve the segmentation in presence of pathological lesions. To improve the segmentation result, we apply some processes which have been discussed in the next section.

4.2 Proposed Approach

We improve the result of segmentation by removing false detected pixels in presence of pathological lesions or other non-vessel pixels. For this improvement, we extract features from the retinal image, train a classifier model and classify the pixels of a test image as vessel or non-vessel. To extract trainable feature from retinal image, we propose a descriptor, **Local Haar Pattern (LHP)** based Haar feature. The proposed descriptor is as follows:

4.2.1 Local Haar Pattern (LHP)

Local Haar Pattern (LHP) is inspired by the earlier works of Saha et al. in [20]. In [20], it was shown that image patches could be effectively described on the basis of a relatively small number of pair-wise intensity comparisons, where Haar features were used to define the pixels group for intensity comparisons. Rather than comparing the intensity of two groups of pixels to generate one bit of the descriptor as in [13], in this work, we compute and store the actual intensity difference, which is to some extent similar to Speeded Up Robust Feature (SURF) [14] where image gradients that relies on intensity difference among subsequent pixels are computed. As in [20], there are many motivations for using features rather than pixels directly. The most common reason is that features can act to encode ad-hoc domain knowledge that is difficult to learn otherwise. In order to perform pixels grouping, we define a set of 16-pixel patterns depicted in Figure 4.6, which are reminiscent of Haar basis function [21].

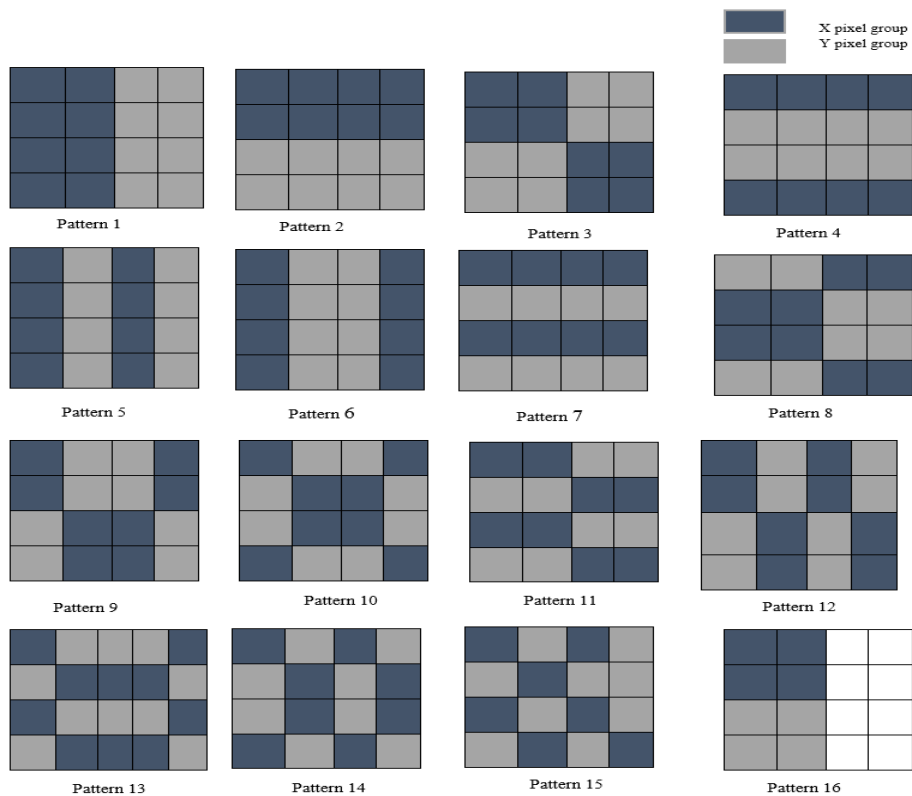


Figure 4.6: All 16 Patterns for feature extraction in LHP

In order to compute the LHP descriptor a patch p of size 32×32 is considered around the pixel of interest, and vector of size 128 bytes is calculated that represents the patch. Each byte of the vector is computed based on the intensity comparisons of two-pixel groups as defined below:

$$T(p, X, Y) = \bar{I}_X - \bar{I}_Y \quad (4.1)$$

where \bar{I}_X and \bar{I}_Y represent the mean intensities of two different pixel groups X and Y belonging to the patch p .

128 bytes vector is generated in three steps. At the first step, all the 16 patterns of Figure 4.6 are considered to perform intensity comparisons on the whole patch, that results 16 bytes vector. In the second step, the patch is divided into 4 sub-patches of size 16×16 . All the 16 patterns are considered and intensity comparisons are performed on each of these sub-patches, which results 64 ($=4 \times 16$) bytes vector. In third stage, each of the sub-patches is further divided into 4 sub-patches of size 8×8 and the first three patterns of Figure 10 are considered to perform intensity comparisons, which results 48 ($=16 \times 3$)- bytes vector.

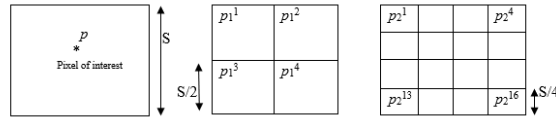


Figure 4.7: Decomposition of main patch into sub-patches

All these vectors are concatenated at the end and a feature vector of size **128-bytes** is formed. Finally, the feature vector is normalized and LHP descriptor is formed.

4.2.2 Training Phase

In this section, we describe the process of extracting trainable features and training the classifier.

4.2.2.1 Extraction of Trainable Feature

We use LHP (Local Haar Pattern) descriptor to extract the features from retinal image. For a given image, at first, we define the interest points for which LHP will extract feature. The descriptor provides 128-bytes feature for each interest points. The details process of generating 128-bytes feature have been discussed in previous sub-section 4.2.1.

For training purpose, we add an extra column to the 128-byte feature vector. We insert the class (vessel or non-vessel) for the corresponding pixels in the column by denoting logical '0' for non-vessel class and logical '1' for vessel class. Finally, 129-dimension (129D) feature vectors are generated and fed to the classifier. We have used the images from DRIVE, STARE, CHASE_DB dataset for training the classifier.

We also use SURF (speeded up robust features) descriptors [14] to compare with the LHP descriptor. For a given image, at first SURF finds the interest points. Then this provides 64-dimensional (64D) feature for each interest points. The details processes of generating interest points and 64D features have been discussed in section 3.2.

4.2.2.2 Training Classifier Model

We use Random Forest (RF) model as a classifier. Random forest is an ensemble which generates multiple decision trees from the input feature vector using a random vector sampled independently [22]. Each tree flings a unit vote for the most popular class to classify an input vector [16]. The majority voted class is the final output of RF method. The process of growing trees has been discussed in the section 3.3.

The block diagram of training phase is shown in Figure 4.8:

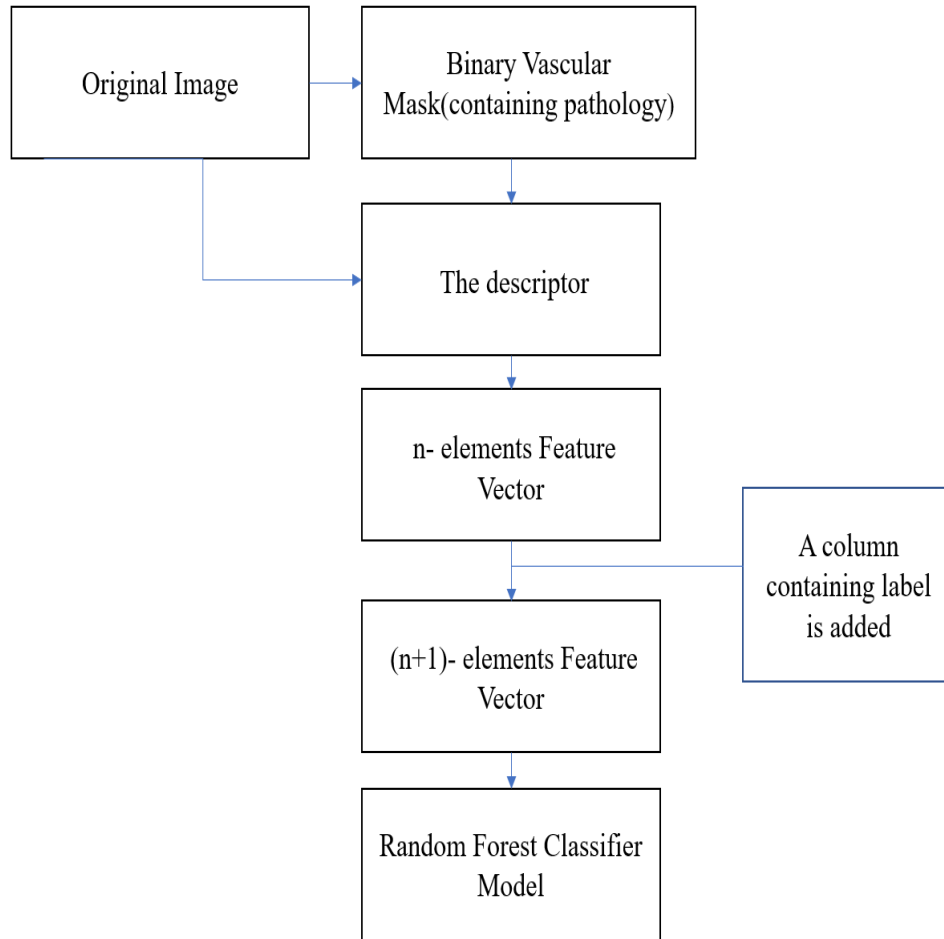


Figure 4.8: Training Phase

4.2.3 Test Phase

For testing a random image, features are fed to the trained model. The steps of test phase are as follows:

1. At first, LPH descriptor is used for extracting 128D features vector. We use the segmented image achieved from the multi-scale line detector as input of the SURF descriptor. The features vector of 128D is provided as output of LPH descriptor. The segmented image contains vessels (actual vessel pixels as well as misclassified vessels) pixels and background pixels. We only extract features for the vessel pixels.
2. Secondly, the features vector of 128D of a test segmented image is fed to Random Forest for prediction. If the prediction result is '1', then pixel is vessel and location

of the pixels will be stored. If the prediction result is '0', then the pixel is simply neglected.

We perform similar process for SURF descriptor. Note that, SURF descriptor provides 64D feature vector.

The block diagram of test phase is given in figure 4.9

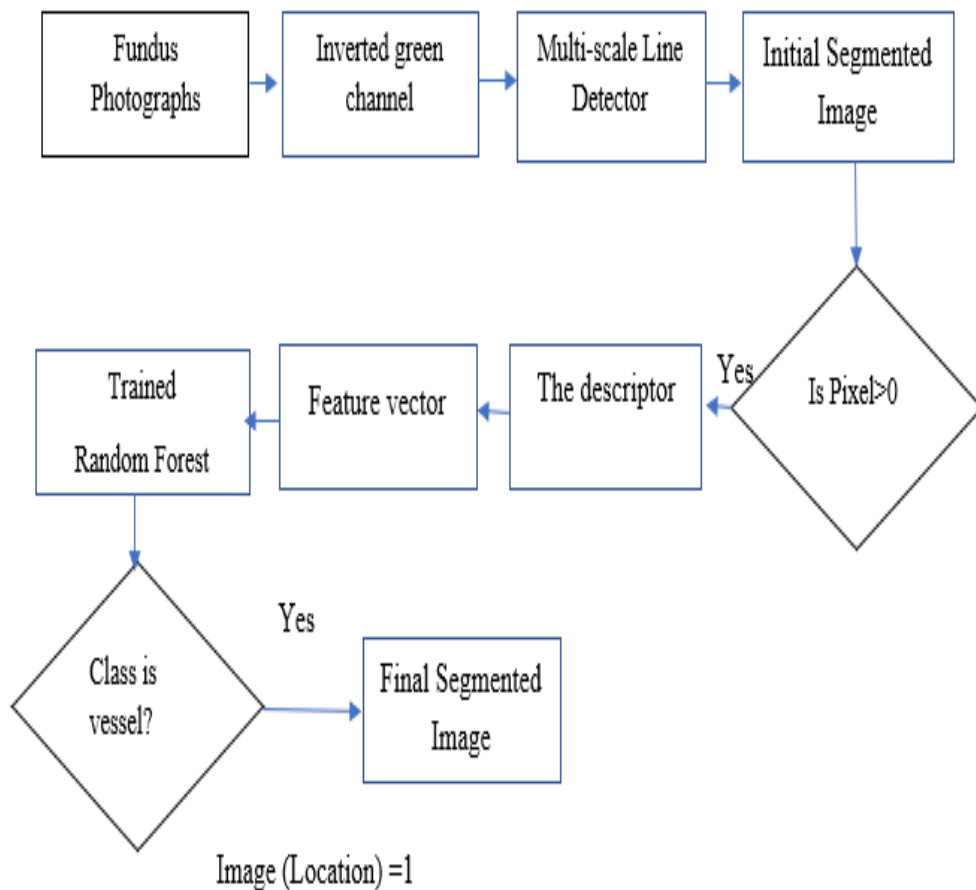


Figure 4.9: Test Phase

Figure 4.10 shows some example of output of the proposed method. We store the location of predicted class of the vessel pixels and the size of the original image. We put pixel value '1' in the stored locations and pixel value '0' in rest of the locations. In this way, we get image without false vessel in presence of pathological lesion in the input image.

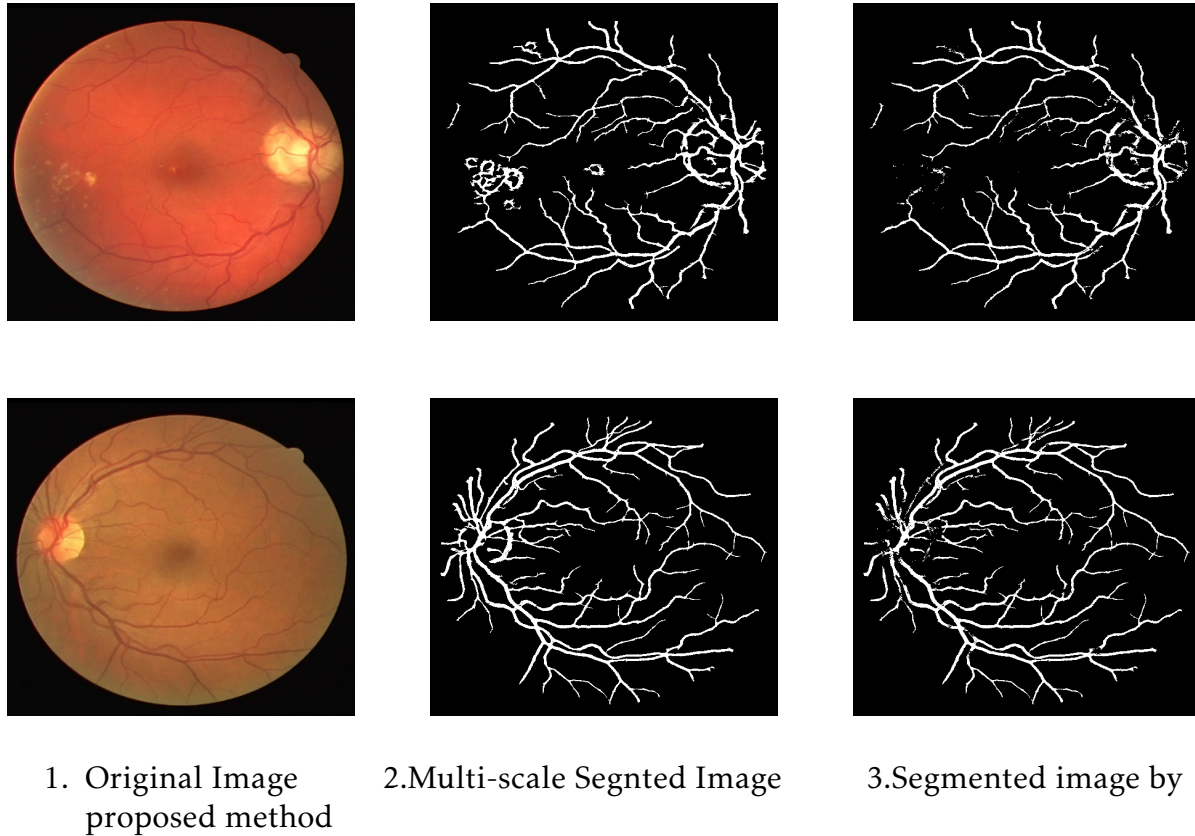


Figure 4.10: Sample output of Proposed Method (LPH descriptor)

Chapter 5

Results and Comparisons

5.1 Model Evaluation on DRIVE Dataset

We have trained the proposed model by twelve images of DRIVE dataset. We have tested the model using four images of the dataset. The Accuracy, Area under Curve, Sensitivity and Specificity are 0.959, 0.840, 0.698 and 0.982 respectively. The performance measure of the proposed method for DRIVE dataset for LHP descriptor has given in Table5.1.

5.2 Model evaluation on STARE dataset

We have trained the proposed model by using twelve images of STARE dataset. Also, we have tested the model using four images of this dataset. The Accuracy, Area Under Curve, Sensitivity, Specificity of the method for STARE dataset are 0.964, 0.889, 0.804, 0.977 respectively. The performance measure of our proposed method for STARE dataset for LHP descriptor has given in Table 5.2.

5.3 Model evaluation on CHASE_DB1 dataset

We have trained the proposed model by using twelve images of CHASE_DB1. Also, we have tested the model using four images of this dataset. The Accuracy, Area Under Curve, Sensitivity, Specificity of the method for CHASE_DB1 dataset for LHP are 0.954, 0.860, 0.751, 0.969 respectively. The performance measure of our proposed method for CHASE_DB1 dataset for LHP descriptor has given in Table5.3.

Table 5.1: Performance results of DRIVE dataset

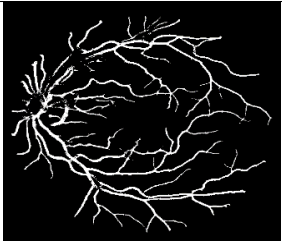
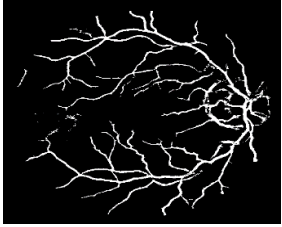
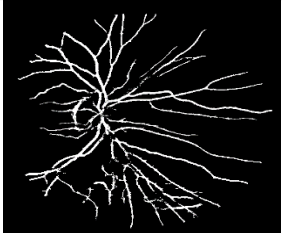
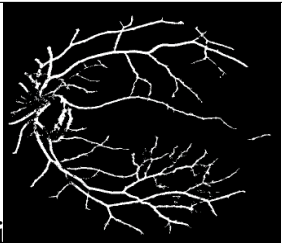
Image title	Segmented image by proposed Method	Performance			
		Accuracy	Area Under Curve (AUC)	Sensitivity	Specificity
01_test.tif		0.963	0.870	0.756	0.983
08_test.tif		0.956	0.820	0.653	0.984
15_test.tif		0.964	0.858	0.733	0.982
26_training.tif		0.959	0.842	0.702	0.983
Average		0.961	0.847	0.711	0.983

Table 5.2: Performance results of STARE dataset

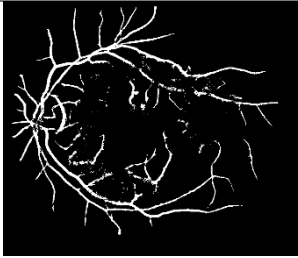
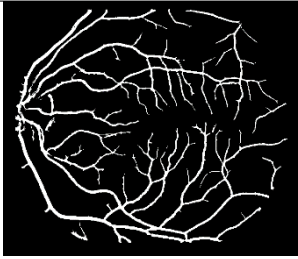
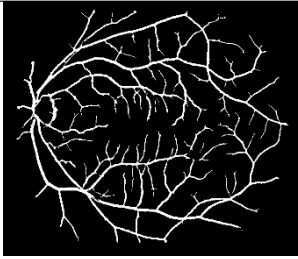
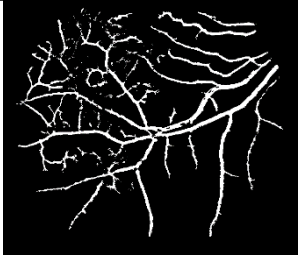
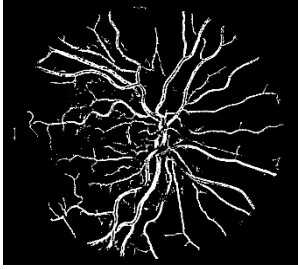
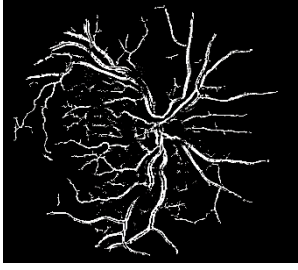
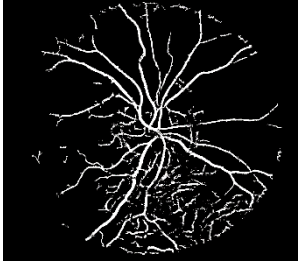
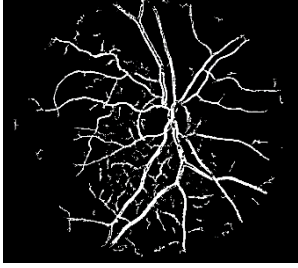
Image title	Segmented image by proposed Method	Performance			
		Accuracy	Area Under Curve (AUC)	Sensitivity	Specificity
Im0002		0.956	0.801	0.623	0.979
Im0077		0.967	0.932	0.890	0.973
Im0255		0.968	0.885	0.785	0.985
Im0324		0.944	0.894	0.835	0.952
Average		0.960	0.878	0.790	0.973

Table 5.3: Performance results of CHASE_DB1 dataset

Image title	Segmented image by proposed Method	Performance			
		Accuracy	Area Under Curve (AUC)	Sensitivity	Specificity
Image_05R		0.952	0.841	0.707	0.975
Image_06R		0.947	0.820	0.671	0.969
Image_09R		0.953	0.878	0.794	0.962
Image_11R		0.952	0.879	0.797	0.961
Average		0.951	0.854	0.742	0.967

The proposed model is compared with other state-of-the art methods on two most popular public datasets (1) DRIVE and (2) STARE. We did not use CHASE_DB1 dataset to compare with other methods. Because, it is recently introduced and there are only few results in the literature. Performance comparison of vessel segmentation methods on Drive and STARE images is shown in Table 5.4:

Table 5.4: Performance comparison on DRIVE and STARE datasets

Methods	Dataset							
	Drive				Stare			
	Acc	AUC	SE	SP	ACC	AUC	SE	SP
Supervised Methods								
Steal et al.[23]	.944	–	–	–	.052	–	–	–
Soares et al.[24]	.946	–	–	–	.948	–	–	–
Lusaces et al.[25]	.959	–	.720	–	–	–	–	–
Marin et al.[11]	.945	.843	.706	.980	.952	–	–	–
Roychowdhury et al.[26]	.952	.844	.725	.962	.951	.873	.772	.973
Liskowski et al.[27]	.954	.881	.781	.981	.973	.921	.855	.986
Unsupervised Methods								
Hoover et al.[28]	–	–	–	–	.928	.730	.650	.810
Mendoca et al.[29]	.945	.855	.734	.976	.944	.836	.699	.973
Lam et al.[30]	–	–	–	–	.947	–	–	–
Al-Diri et al.[31]	–	–	.728	.955	–	–	.752	.968
Lam and Yan et al.[32]	.947	–	–	–	.957	–	–	–
Perez et al.[33]	.925	.806	.644	.967	.926	.857	.769	.944
Miri et al.[34]	.943	.846	.715	.976	–	–	–	–
Budai et al.[35]	.957	.816	.644	.987	.938	.781	.580	.982
Yitian et al.[36]	.954	.862	.742	.982	.956	.874	.780	0.978
Annunziata et al.[37]	–	–	–	–	.956	.849	.731	.984
Orlando et al.[38]	–	.879	.790	.968	–	.871	.768	.974
Nyugen et al [4]	.941	–	–	–	0.932	–	–	–
Proposed	.959	.840	.698	.982	.964	.889	.804	.977

In table 5.4, we have showed the performance measures of some state-of-the-art papers. From the table, it is showed that our proposed method provides higher accuracy than the other methods for DRIVE dataset except the method of Lupascu et.al [25]. The accuracy of both methods is 0.959. The obtained accuracy is also significant for the STARE dataset. The method of Liskowski et.al [27] only showed the higher accuracy than our method. We also get the promising Sensitivity, Specificity and Area Under Curve (AUC). The Accuracy, Sensitivity, Specificity and AUC of Marin et al [11] are 0.945, 0.706, 0.980 and 0.843 respectively for DRIVE dataset. The proposed method has showed better performance for all parameter than Marin et Al [11] method for DRIVE dataset as well as STARE dataset. Stall et al [23] method showed the Accuracy of 0.944 and 0.952 for DRIVE and STARE dataset respectively. Also, in this case, the proposed method has performed well. The comparative performance of the proposed method is given below as charts:

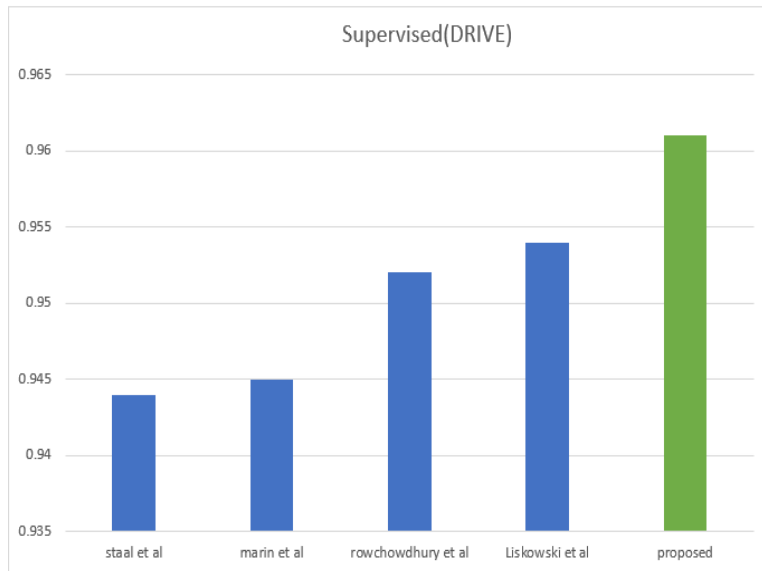


Figure 5.1: Performance comparison on DRIVE dataset (Supervised)

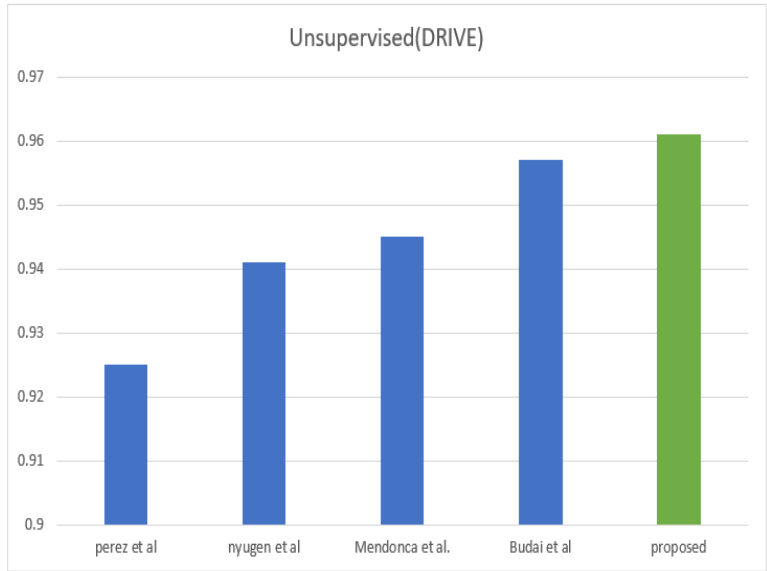


Figure 5.2: Performance comparison on DRIVE dataset (Un-supervised)

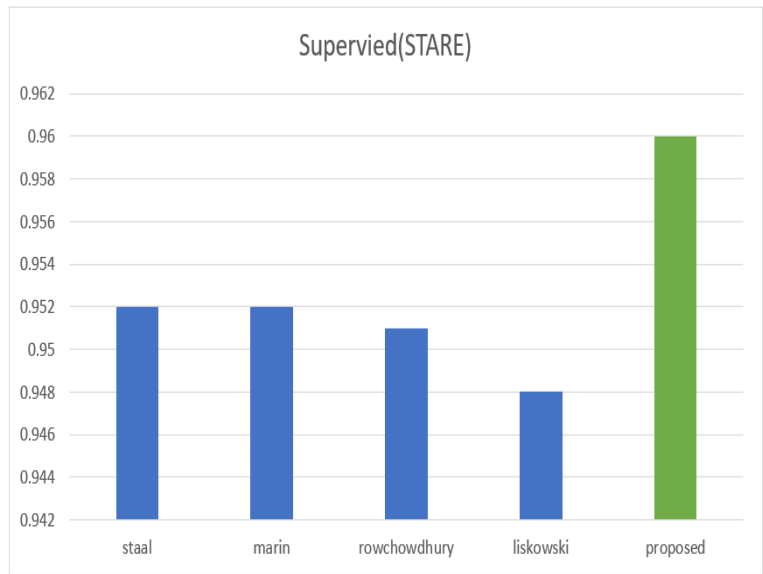


Figure 5.3: Performance comparison on Stare dataset (Supervised)

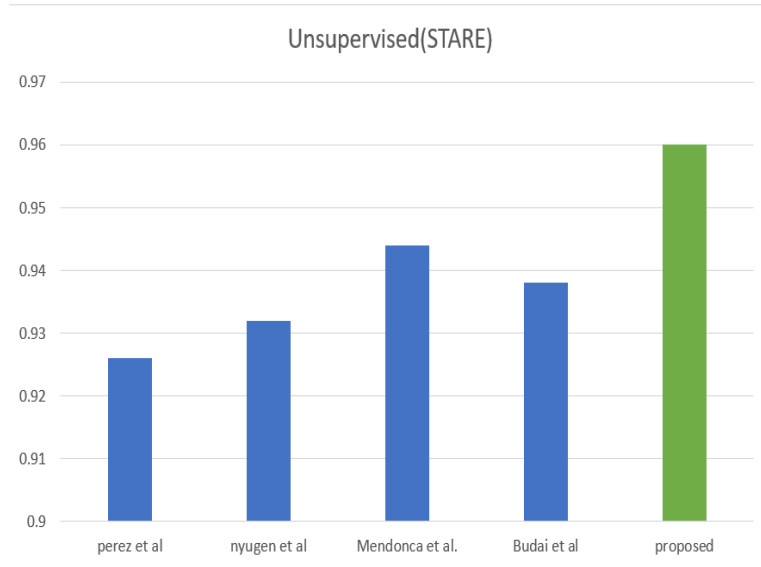


Figure 5.4: Performance comparison on Stare dataset (Un-supervised)

In this thesis, we improve the vessel segmentation method proposed by Nyugen et al. [4] by removing the false detected vessels. In most of the cases, we are able to improve the accuracy than the Nyugen proposed method. We are also able to remove the false vessels. The obtained accuracy of the Nyugen [4] method are 0.941 and 0.932 for DRIVE and STARE datasets respectively. On the other hand, the obtained accuracy of the proposed method is 0.961 and 0.960 for DRIVE and STARE dataset respectively. It is noteworthy that, we evaluated the proposed method on CHASE_DB1 dataset and got promising performance. Comparison with the Nyugen’s method is shown in following chart:

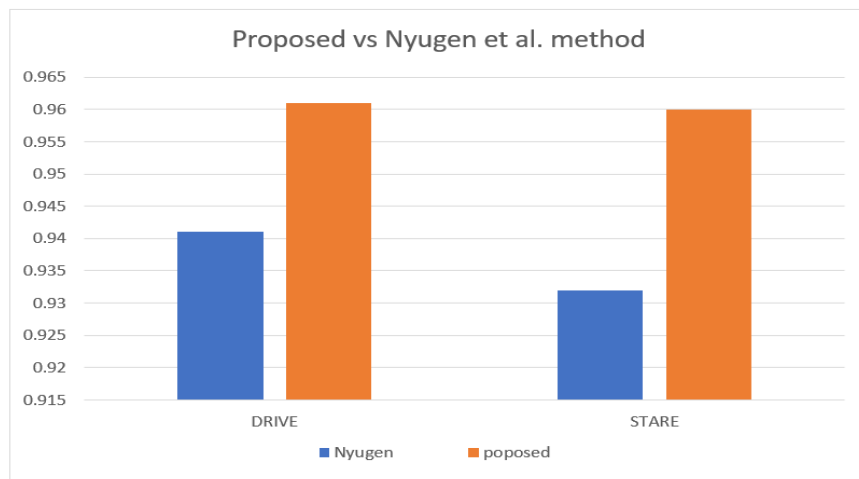


Figure 5.5: Performance comparison of proposed and Nyugen et al.

We compare our proposed descriptor (LHP) with SURF which is one of the powerful and widely used descriptor. The comparative performance is shown in table 5.5. The performance of SURF and LHP is very identical. However, we have taken the 16 patterns randomly to calculate the feature. Here, optimization may be performed by taking the patterns more relevant to the retinal image segmentation. Thus, quality of feature as well as performance of LHP should be improved. On the other hand, the SURF is already optimized. So, there is rare possibility to improve the performance of SURF.

Table 5.5: Comparative performance of Descriptors

Descriptors	Dataset								
	DRIVE			STARE			CHASE_DB1		
	Acc	Sen	Sp	Acc	Sen	Sp	Acc	Sen	Sp
SURF	0.961	0.737	0.981	0.960	0.805	0.972	0.955	0.763	0.969
LHP (pro- posed)	0.961	0.711	0.983	0.960	0.783	0.973	0.951	0.742	0.967

Chapter 6

Conclusion

In this thesis, we proposed a semi-supervised method to segment retinal blood vessels in color fundus photographs. In unsupervised part, we have used multi-scale line detector for segmenting retinal images that may contain false vessels. Then we have used supervised technique to remove false vessels from initial segmented image. SURF descriptor has been used to extract trainable feature and Random Forest (RF) Classifier model has been used for classifying vessel or non-vessel pixel. The method is validated using three publicly available datasets: DRIVE, STARE and CHASE_DB1. The overall accuracy is 0.961, 0.960 and 0.951 for DRIVE, STARE and CHASE_DB1 datasets respectively. The proposed method has shown promising accuracy for the retinal image containing pathology. The method has shown less (sometimes equal) than multi-scale line detector for the normal retinal images. Because, few vessels are misclassified as non-vessels. But it is noted that the number of misclassified pixels is not significant. So, the proposed method is capable of removing false vessels in presence of pathological lesions and also preserves the actual segmentation of vessel pixels.

References

- [1] Agurto, Carla, Victor Murray, Eduardo Barriga, Sergio Murillo, Marios Pattichis, Herbert Davis, Stephen Russell, Michael Abràmoff, and Peter Soliz. "Multiscale AM-FM methods for diabetic retinopathy lesion detection." *IEEE transactions on medical imaging* 29, no. 2 (2010): 502-512.
- [2] Sadek, Ibrahim, Désiré Sidibé, and F. Meriaudeau. "Automatic discrimination of color retinal images using the bag of words approach." In *Medical Imaging 2015: Computer-Aided Diagnosis*, vol. 9414, p. 94141J. International Society for Optics and Photonics, 2015.
- [3] <https://www.isi.uu.nl/Research/Databases/DRIVE/> (accessed July 08, 2018).
- [4] Nguyen, Uyen TV, Alauddin Bhuiyan, Laurence AF Park, and Kotagiri Ramamohanarao. "An effective retinal blood vessel segmentation method using multi-scale line detection." *Pattern recognition* 46, no. 3 (2013): 703-715.
- [5] https://en.wikipedia.org/wiki/Diabetic_retinopathy/ (accessed July 05, 2018).
- [6] Srinidhi, Chetan L., P. Aparna, and Jeny Rajan. "Recent advancements in retinal vessel segmentation." *Journal of medical systems* 41, no. 4 (2017): 70.
- [7] Wang, Yangfan, Guangrong Ji, Ping Lin, and Emanuele Trucco. "Retinal vessel segmentation using multiwavelet kernels and multiscale hierarchical decomposition." *Pattern Recognition* 46, no. 8 (2013): 2117-2133.
- [8] Dash, Jyotiprava, and Nilamani Bhoi. "A thresholding-based technique to extract retinal blood vessels from fundus images." *Future Computing and Informatics Journal* 2, no. 2 (2017): 103-109.
- [9] Yang, Yong, Shuying Huang, and Nini Rao. "An automatic hybrid method for retinal blood vessel extraction." *International Journal of Applied Mathematics and Computer Science* 18, no. 3 (2008): 399-407.
- [10] Wang, Shuangling, Yilong Yin, Guibao Cao, Benzhenq Wei, Yuanjie Zheng, and Gongping Yang. "Hierarchical retinal blood vessel segmentation based on feature and ensemble learning." *Neurocomputing* 149 (2015): 708-717.

- [11] Marín, Diego, Arturo Aquino, Manuel Emilio Gegúndez-Arias, and José Manuel Bravo. "A new supervised method for blood vessel segmentation in retinal images by using gray-level and moment invariants-based features." *IEEE transactions on medical imaging* 30, no. 1 (2011): 146.
- [12] Ricci, Elisa, and Renzo Perfetti. "Retinal blood vessel segmentation using line operators and support vector classification." *IEEE transactions on medical imaging* 26, no. 10 (2007): 1357-1365.
- [13] Lowe, David G. "Object recognition from local scale-invariant features." In *Computer vision, 1999. The proceedings of the seventh IEEE international conference on*, vol. 2, pp. 1150-1157. Ieee, 1999.
- [14] Bay, Herbert, Andreas Ess, Tinne Tuytelaars, and Luc Van Gool. "Speeded-up robust features (SURF)." *Computer vision and image understanding* 110, no. 3 (2008): 346-359.
- [15] Khan, Nabeel Younus, Brendan McCane, and Geoff Wyvill. "SIFT and SURF performance evaluation against various image deformations on benchmark dataset." In *2011 International Conference on Digital Image Computing: Techniques and Applications*, pp. 501-506. IEEE, 2011.
- [16] Breiman, Leo. "Random forests." *Machine learning* 45, no. 1 (2001): 5-32.
- [17] <http://cecas.clemson.edu/~ahoover/stare/> (accessed Nov 29, 2018).
- [18] <https://blogs.kingston.ac.uk/retinal/chasedb1/> (accessed 15 November,2018)
- [19] Fan, Zhun, Jiewei Lu, Wenji Li, Caimin Wei, Han Huang, Xinye Cai, and Xinjian Chen. "A Hierarchical Image Matting Model for Blood Vessel Segmentation in Fundus images." *arXiv preprint arXiv:1701.00892* (2017).
- [20] Saha, Sajib, and Vincent Démoulin. "ALOHA: An efficient binary descriptor based on Haar features." In *Image Processing (ICIP), 2012 19th IEEE International Conference on*, pp. 2345-2348. IEEE, 2012.
- [21] Viola, Paul, and Michael Jones. "Rapid object detection using a boosted cascade of simple features." In *Computer Vision and Pattern Recognition, 2001. CVPR 2001. Proceedings of the 2001 IEEE Computer Society Conference on*, vol. 1, pp. I-I. IEEE, 2001.
- [22] Pal, Mahesh. "Random forest classifier for remote sensing classification." *International Journal of Remote Sensing* 26, no. 1 (2005): 217-222.
- [23] Staal, Joes, Michael D. Abramoff, Meindert Niemeijer, Max A. Viergever, and Bram Van Ginneken. "Ridge-based vessel segmentation in color images of the retina." *IEEE transactions on medical imaging* 23, no. 4 (2004): 501-509.

- [24] Soares, João VB, Jorge JG Leandro, Roberto M. Cesar, Herbert F. Jelinek, and Michael J. Cree. "Retinal vessel segmentation using the 2-D Gabor wavelet and supervised classification." *IEEE Transactions on medical Imaging* 25, no. 9 (2006): 1214-1222.
- [25] Lupascu, Carmen Alina, Domenico Tegolo, and Emanuele Trucco. "FABC: retinal vessel segmentation using AdaBoost." *IEEE Transactions on Information Technology in Biomedicine* 14, no. 5 (2010): 1267-1274.
- [26] Roychowdhury, Sohini, Dara D. Koozekanani, and Keshab K. Parhi. "Blood vessel segmentation of fundus images by major vessel extraction and subimage classification." *IEEE journal of biomedical and health informatics* 19, no. 3 (2015): 1118-1128.
- [27] Liskowski, Paweł, and Krzysztof Krawiec. "Segmenting retinal blood vessels with deep neural networks." *IEEE transactions on medical imaging* 35, no. 11 (2016): 2369-2380.
- [28] Hoover, A. D., Valentina Kouznetsova, and Michael Goldbaum. "Locating blood vessels in retinal images by piecewise threshold probing of a matched filter response." *IEEE Transactions on Medical imaging* 19, no. 3 (2000): 203-210.
- [29] Mendonca, Ana Maria, and Aurelio Campilho. "Segmentation of retinal blood vessels by combining the detection of centerlines and morphological reconstruction." *IEEE transactions on medical imaging* 25, no. 9 (2006): 1200-1213.
- [30] Lam, Benson Shu Yan, and Hong Yan. "A novel vessel segmentation algorithm for pathological retina images based on the divergence of vector fields." *IEEE Transactions on Medical Imaging* 27, no. 2 (2008): 237-246.
- [31] Al-Diri, Bashir, Andrew Hunter, and David Steel. "An active contour model for segmenting and measuring retinal vessels." *IEEE Transactions on Medical imaging* 28, no. 9 (2009): 1488-1497.
- [32] Lam, Benson SY, Yongsheng Gao, and Alan Wee-Chung Liew. "General retinal vessel segmentation using regularization-based multiconcavity modeling." *IEEE Transactions on Medical Imaging* 29, no. 7 (2010): 1369-1381.
- [33] Palomera-Pérez, Miguel A., M. Elena Martínez-Pérez, Hector Benítez-Pérez, and Jorge Luis Ortega-Arjona. "Parallel multiscale feature extraction and region growing: application in retinal blood vessel detection." *IEEE transactions on information technology in biomedicine* 14, no. 2 (2010): 500-506.
- [34] Miri, Mohammad Saleh, and Ali Mahloojifar. "Retinal image analysis using curvelet transform and multistructure elements morphology by reconstruction." *IEEE Transactions on Biomedical Engineering* 58, no. 5 (2011): 1183-1192.

- [35] Budai, Attila, Rüdiger Bock, Andreas Maier, Joachim Hornegger, and Georg Michelson. "Robust vessel segmentation in fundus images." *International journal of biomedical imaging* 2013 (2013).
- [36] Zhao, Yitian, Lavdie Rada, Ke Chen, Simon P. Harding, and Yalin Zheng. "Automated Vessel Segmentation Using Infinite Perimeter Active Contour Model with Hybrid Region Information with Application to Retinal Images." *IEEE Trans. Med. Imaging* 34, no. 9 (2015): 1797-1807.
- [37] Annunziata, Roberto, Andrea Garzelli, Lucia Ballerini, Alessandro Mecocci, and Emanuele Trucco. "Leveraging multiscale hessian-based enhancement with a novel exudate inpainting technique for retinal vessel segmentation." *IEEE journal of biomedical and health informatics* 20, no. 4 (2016): 1129-1138.
- [38] Orlando, José Ignacio, Elena Prokofyeva, and Matthew B. Blaschko. "A discriminatively trained fully connected conditional random field model for blood vessel segmentation in fundus images." *IEEE Transactions on Biomedical Engineering* 64, no. 1 (2017): 16-27.